Particle Spectroscopy of Supersymmetric SU(5) in Light of 125 GeV Higgs and Muon $g-2$ Data

Nobuchika Okada[a,1], Shabbar Raza [b,2] and Qaisar Shafi [b,3]

[a] *Department of Physics and Astronomy, University of Alabama, Tuscaloosa, Alabama 35487, USA*
[b] *Bartol Research Institute, Department of Physics and Astronomy, University of Delaware, Newark, DE 19716, USA*

arXiv:1307.0461v1 [hep-ph] 1 Jul 2013

Abstract

The discovery of the Higgs boson at the Large Hadron Collider (LHC) has a great impact on the minimal supersymmetric extension of the Standard Model (MSSM). In the context of the constrained MSSM (CMSSM) and its extension with non-universal masses for the MSSM Higgs doublets (NUHM2), sparticles with masses > 1 TeV are necessary to reproduce the observed Higgs boson mass of 125-126 GeV. On the other hand, there appears to be a significant amount of discrepancy between the measured muon $g-2$ and the Standard Model prediction. A successful explanation of this discrepancy in the MSSM requires new contributions involving relatively light sparticles with masses < 1 TeV. In this paper, we attempt to accommodate the two conflicting requirements in an SU(5) inspired extension of the CMSSM. We assign non-universal but flavor blind soft supersymmetry breaking masses to the scalar components in $\bar{5}$ and 10 matter supermultiplets. The two MSSM Higgs doublets in the 5, $\bar{5}$ representations of $SU(5)$ are also assigned unequal soft mass^2 at M_{GUT}. We identify parameter regions which can simultaneously accommodate the observed Higgs boson mass and the muon $g-2$ data, and which are compatible with other phenomenological constraints such as neutralino dark matter relic abundance and rare B-meson decays. Some regions of the allowed parameter space will be explored at the upgraded LHC and by dark matter direct detection experiments.

[1] Email: okadan@ua.edu
[2] Email: shabbar@udel.edu. On study leave from: Department of Physics, FUUAST, Islamabad, Pakistan.
[3] Email: shafi@bartol.udel.edu.

1 Introduction

By resolving the gauge hierarchy problem, supersymmetry (SUSY) is a prime candidate for new physics beyond the Standard Model (SM). The MSSM predicts a plethora of new particles in the TeV mass range. Under the assumption of R-parity conservation, the lightest supersymmetric particle (LSP) neutralino is a very plausible dark matter candidate. The electroweak symmetry is radiatively broken by the interplay between the soft SUSY breaking masses and the large top Yukawa coupling. The quartic Higgs coupling is determined by the electroweak gauge couplings and as a result, the SM-like Higgs boson mass is predicted in terms of the scalar top quark masses and other soft SUSY breaking parameters. Furthermore, in the MSSM with SUSY broken at the TeV scale, the three SM gauge couplings successfully unify at the grand unified theory (GUT) scale, $M_{\rm GUT} \simeq 2 \times 10^{16}$ GeV. This fact strongly supports the GUT paradigm that the three SM gauge interactions are unified within a gauge group such as SU(5) or SO(10).

The recent discovery of the SM-like Higgs boson by the ATLAS [1] and CMS [2] collaborations at the Large Hadron Collider (LHC) has several important implications for the MSSM, along with other phenomenological constraints. Following this discovery, the sparticle mass spectroscopy has been intensively studied, in particular, in light of the observed Higgs boson of mass around 125 GeV [3]. Since the MSSM tree-level prediction for the SM-like Higgs boson is below the Z-boson mass, a significant enhancement of the Higgs boson mass is achieved through quantum corrections involving the stops. In the context of the CMSSM and its extension contains non-universal masses of the MSSM Higgs doublets (NUHM), it has been found that the sfermions are as heavy as $1 - 10$ TeV [3].

On the other hand, there is some indication of new physics beyond the SM stemming from muon $g-2$ ($a_\mu = (g_\mu - 2)/2$), which has been precisely measured by the BNL experiment [4]. The data shows a discrepancy from the SM prediction (a_μ^{SM}) [5], namely

$$2.1 \times 10^{-10} \leq \Delta a_\mu \leq 50.1 \times 10^{-10}\ (3\sigma), \tag{1}$$

where $\Delta a_\mu = a_\mu^{\rm exp} - a_\mu^{SM}$. This indicates new physics beyond the SM, and the MSSM with relatively light sleptons, neutralinos and charginos is a primary candidate to account for the discrepancy [6]. Unfortunately, because of the heavy sparticles the CMSSM and NUHM fail to resolve this discrepancy.

In this paper, we attempt to reconcile the muon $g-2$ data with other phenomenological constraints on the MSSM, such as realizing a SM-like Higgs boson mass of 125-126 GeV, Wilkinson Microwave Anisotropy Probe (WMAP9) [26] and Planck2013 [27] compatible neutralino dark matter abundance in a generalized CMSSM inspired by SU(5) GUT [7]. The standard CMSSM assumes universality of scalar masses, the gaugino masses and the A-parameters. Motivated by SU(5) GUT, we do not require

universal masses at $M_{\rm GUT}$ for the $\bar{5}$ and 10 matter multiplets (flavor universal masses are assumed). The GUT scale boundary conditions for (flavor universal) soft SUSY breaking (SSB) sfermion masses are as follows:

$$\begin{aligned} m_{\tilde{D}^c} &= m_{\tilde{L}} = m_{\bar{5}}, \\ m_{\tilde{Q}} &= m_{\tilde{U}^c} = m_{\tilde{E}^c} = m_{10}. \end{aligned} \tag{2}$$

As in the NUHM2, the masses for the MSSM Higgs doublets are taken as free parameters, since they reside in 5 and $\bar{5}$ multiplets under SU(5). The remaining parameters are the same as in the CMSSM. Clearly, the NUHM2 case can be realized by setting $m_{\bar{5}} = m_{10}$. With this set of free parameters, we perform a random parameter scan under a variety of phenomenological constraints and identify parameter regions which satisfy the imposed constraints as well as the SUSY explanation of the muon $g-2$ data. For a similar discussion but with non-universal gaugino mass models, see [8]. See also [9] for a discussion with the gauge mediation.

2 Phenomenological constraints and scanning procedure

We employ the ISAJET 7.84 package [10] to perform random scans over the parameter space in the generalized CMSSM inspired by SU(5) GUT. In this package, the weak scale values of gauge and third generation Yukawa couplings are evolved to $M_{\rm GUT}$ via the MSSM renormalization group equations (RGEs) in the $\overline{DR}$ regularization scheme. We do not strictly enforce the unification condition $g_3 = g_1 = g_2$ at $M_{\rm GUT}$, since a few percent deviation from unification can be assigned to unknown GUT-scale threshold corrections [11]. With the boundary conditions given at $M_{\rm GUT}$, all the SSB parameters, along with the gauge and Yukawa couplings, are evolved back to the weak scale $M_{\rm Z}$.

In evaluating Yukawa couplings the SUSY threshold corrections [13] are taken into account at the common scale $M_{\rm SUSY} = \sqrt{m_{\tilde{t}_L} m_{\tilde{t}_R}}$. The entire parameter set is iteratively run between $M_{\rm Z}$ and $M_{\rm GUT}$ using the full 2-loop RGEs until a stable solution is obtained. To better account for leading-log corrections, one-loop step-beta functions are adopted for gauge and Yukawa couplings, and the SSB parameters m_i are extracted from RGEs at appropriate scales $m_i = m_i(m_i)$. The RGE-improved 1-loop effective potential is minimized at an optimized scale $M_{\rm SUSY}$, which effectively accounts for the leading 2-loop corrections. Full 1-loop radiative corrections are incorporated for all sparticle masses.

The requirement of radiative electroweak symmetry breaking (REWSB) [14] puts an important theoretical constraint on the parameter space. Another important

constraint comes from limits on the cosmological abundance of stable charged particles [15]. This excludes regions in the parameter space where charged SUSY particles, such as $\tilde{\tau}_1$ or $\tilde{t}_1$, become the LSP. We accept only those solutions for which one of the neutralinos is the LSP and saturates the dark matter relic abundance bound observed by WMAP9 and Planck2013.

We have performed Markov-chain Monte Carlo (MCMC) scans for the following parameter range:

$$\begin{aligned} 0 \leq m_{\bar{5}} &\leq 2\,\text{TeV} \\ 0 \leq m_{10} &\leq 10\,\text{TeV} \\ 0 \leq M_{1/2} &\leq 2\,\text{TeV} \\ 0 \leq \mu &\leq 2\,\text{TeV} \\ 0 \leq m_A &\leq 2\,\text{TeV} \\ A_0 &= -6, -5, -4, -3, 0, 4\,\text{TeV} \\ \tan\beta &= 10, 30, 50, \end{aligned} \tag{3}$$

with $\mu > 0$ and $m_t = 173.3\,\text{GeV}$ [16]. Note that our results are not too sensitive to one or two sigma variation in the value of m_t [17]. We use $m_b^{\overline{DR}}(M_Z) = 2.83$ GeV which is hard-coded into ISAJET.

In scanning the parameter space, we employ the Metropolis-Hastings algorithm as described in [18]. The data points collected all satisfy the requirement of REWSB, with the neutralino in each case being the LSP. After collecting the data, we impose the mass bounds on all the particles [15] and use the IsaTools package [19, 20] and Ref. [21] to implement the following phenomenological constraints:

$$m_h = 124 - 127 \text{ GeV} \quad [1,\ 2] \tag{4}$$

$$0.8 \times 10^{-9} \leq \text{BR}(B_s \to \mu^+\mu^-) \leq 6.2 \times 10^{-9}\ (2\sigma) \quad [22] \tag{5}$$

$$2.99 \times 10^{-4} \leq \text{BR}(b \to s\gamma) \leq 3.87 \times 10^{-4}\ (2\sigma) \quad [24] \tag{6}$$

$$0.15 \leq \frac{\text{BR}(B_u \to \tau\nu_\tau)_{\text{MSSM}}}{\text{BR}(B_u \to \tau\nu_\tau)_{\text{SM}}} \leq 2.41\ (3\sigma) \quad [25] \tag{7}$$

$$0.0913 \leq \Omega_{\text{CDM}}h^2(\text{WMAP9}) \leq 0.1363\ (5\sigma) \quad [26] \tag{8}$$

$$2.1 \times 10^{-10} \leq \Delta a_\mu \leq 50.1 \times 10^{-10}\ (3\sigma) \quad [4] \tag{9}$$

3 Results

In Fig. 1 we show our results in the $(m_h,\ \Delta a_\mu)$-plane for $A_0 = -3$ TeV, $\tan\beta = 10$, 30 and 50. Gray points satisfy the requirements of REWSB and neutralino LSP. Orange points satisfy the mass bounds and B-physics bounds. Blue points are a subset of orange points and represent solutions satisfying the WMAP9 bounds at

5σ as well as $m_{\tilde{g}},\ m_{\tilde{d}_R} \geq 1$ TeV. The horizontal dashed red and solid black lines represent the central value of Δa_μ and the lower bar of the 3σ variation from the central value respectively. For $\tan\beta = 30$ and 50 and $A_0 = -3$ TeV, only a very limited parameter space can simultaneously satisfy the Higgs boson mass bound and the muon $g-2$ data, while for $\tan\beta = 10$, none of the points can do this. Similar plots with $A_0 = -4$, -5 and -6 TeV, are shown in Figs. 2-4. Analogous to Fig. 1, we find parameter regions for $\tan\beta = 30$ and 50 which are consistent with the Higgs boson mass and the muon $g-2$ bounds. The results for $A_0 = 0$ and 4 TeV are shown in Figs. 5 and 6. For positive A_0 values, no satisfactory solution is found.

In Fig. 7, we present our results in the fundamental parameter space ($m_{\bar{5}}$, m_{10}, $M_{1/2}$, μ and m_A) for $A_0 = -3$ TeV and $\tan\beta = 30$. Gray points satisfy the requirements of REWSB and neutralino LSP. Orange points satisfy, in addition, the mass bounds and B-physics bounds. Blue points are a subset of the orange points and represent solutions satisfying the WMAP9 bounds at 5σ, $124\,\text{GeV} \leq m_h \leq 127\,\text{GeV}$, and $m_{\tilde{g}},\ m_{\tilde{d}_R} \geq 1$TeV. Green points are a subset of the blue points and satisfy the 3σ bound on Δa_μ. In the top-left panel, the black solid line represents the relation $m_{\bar{5}} = m_{10}$. We see that most of the green points appear in the region $m_{\bar{5}} < m_{10}$. In other words, it is quite difficult to stay within the 3σ bound of Δa_μ in the context of CMSSM/NUHM2. The green points appear for $m_{\bar{5}} \lesssim 1.6$ TeV, 1 TeV $\lesssim m_{10} \lesssim 2$ TeV, 1.3 TeV $\lesssim M_{1/2}$, 0.6 TeV $\lesssim \mu \lesssim 0.9$ TeV and 0.8 TeV $\lesssim m_A$. The results for different values of $A_0 = -4$, -5, -6 TeV are depicted in Figs. 8-12. We see that our results are more or less similar to those in Fig. 7. However, note that for $A_0 = -4$, -5, -6 TeV, the condition $m_{\bar{5}} < m_{10}$ is necessary to have green points. In all figures, the Higgsino mass parameter is always found to be relatively small, namely $\mu = 0.6 - 0.8$ TeV for most of the green points.

In Fig. 13 we present our results for $A_0 = -3$ TeV and $\tan\beta = 30$ in terms of sparticle masses: LSP neutralino $m_{\tilde{\chi}_1^0}$, lighter stau $m_{\tilde{\tau}_1}$, lighter chargino $m_{\tilde{\chi}_1^\pm}$, lighter sneutrino $m_{\tilde{\nu}_3}$, and CP-odd Higgs boson m_A. Here the color coding is the same as in Fig 7. The solid lines represent the mass degeneracy of the LSP neutralino with the lighter stau, lighter chargino and lighter sneutrino. In the bottom-right panel, the solid line corresponds to the relation $2m_{\tilde{\chi}_1^0} = m_A$. The region 0.6 TeV $\lesssim \mu \lesssim 0.9$ TeV corresponds to $m_{\tilde{\chi}_1^0} = 0.55 - 0.8$ TeV, and we can see from the top-right panel that the neutralino LSP is closely-degenerate in mass with the lighter chargino for most of the green points. A more careful investigation of this region reveals that the neutralino LSP is a bino-Higgsino admixture.

The results for $A_0 = -4$ TeV are depicted in Fig. 14 with the same color coding as in Fig. 7. Here we note from the top-right panel that the neutralino LSP is nearly-degenerate in mass with the lighter chargino for most of the green points. In the top-left and bottom-left panels, we see that the stau and sneutrino are nearly-degenerate with the neutralino LSP. Further investigation shows that for most of

these points, the sneutrino is closer in mass to the neutralino LSP than the stau, and the correct neutralino LSP relic density is realized through the sneutrino-neutralino coannihilation process (the sneutrino-neutralino coannihilation region). However, we also found the stau-neutralino coannihilation region for a limited set of points. In the bottom-right panel, some of the green points lie close to the solid line corresponding to the relation $2m_{\tilde{\chi}_1^0} = m_A$, where the desired neutralino relic abundance is achieved by efficient annihilation processes through the A-resonance (A-resonance region). The results for values of $A_0 = -4$, -5 and -6 TeV and $\tan\beta = 30$ and 50 are shown in Figs. 14-18. We see that they are more or less similar to those in Fig. 13.

For the green points which satisfy all constraints, we also calculate the spin-independent (SI) and spin-dependent (SD) elastic scattering cross sections of the dark matter neutralino with a nucleon, and compare our results with the current and future bounds of direct dark matter detection experiments. In Fig. 19, we show the cross sections for the case with $A_0 = -3$ TeV and $\tan\beta = 30$. The points all satisfy the requirements of REWSB, neutralino LSP, mass bounds, B-physics bounds, the WMAP9 bound, Higgs boson mass and Δa_μ bounds. The purple, green, orange and brown points represent the results, respectively, in the bino-Higgsino mixed dark matter region, the sneutrino-neutralino coannihilation region, the A-resonance and the stau-neutralino coannihilation region. In the left panel, the black line represents the current upper bound set by XENON 100 [28], while the blue (red) line represents the future reach of XENON 1T [29] (SuperCDMS [30]) experiment. In the right panel, the current upper bounds from Super-K [31] (blue line) and the IceCube DeepCore [32] (red line), and the future reach of IceCube DeepCore experiments (black line) are shown. We note that almost all of the purple points (the bino-Higgsino mixed dark matter region) have already been excluded by the current XENON 100 results.

The cross sections for A_0 values of -4, -5 and -6 TeV and $\tan\beta = 30$ and 50 are shown in Figs. 20-24, respectively. Color coding is the same as in Fig. 19. Interestingly, the resultant SI cross sections are large enough to lie within the reach of the future direct dark matter detection experiments (most of the purple points have already been excluded.).

In Fig. 25 we present our results in the ($m_{\tilde{g}}$, $m_{\tilde{d}_R}$)-plane. Gray points satisfy the requirements of REWSB and neutralino LSP. Orange points satisfy the mass and B-physics bounds. Blue points are a subset of the orange points and represent solutions satisfying the WMAP9 (5σ) bounds, 124 GeV $\leq m_h \leq$ 127 GeV, $m_{\tilde{g}}$, $m_{\tilde{d}_R} \gtrsim 1$ TeV. Red points are subset of the blue points and satisfy the 3σ bounds on Δa_μ, and the current upper bounds set by XENON 100. It has been shown in [33] that for $m_{\tilde{q}} \simeq m_{\tilde{g}}$, the LHC14 with 100 fb^{-1} of data will probe $m_{\tilde{g}}$ up to 3 TeV. Therefore, some of our results can be tested in the near future at the LHC. Similar results can be seen for other A_0 and $\tan\beta$ values in Fig 26.

Finally, we select four benchmark points from the results with different values of

A_0 and $\tan\beta$ and show the mass spectrum in Table 1. The first, second, third and fourth columns are taken, respectively, from the stau-neutralino coannihilation region, the bino-Higgsino mixed dark matter region, the sneutrino-neutralino coannihilation region, and the A-resonance region. These points satisfy all phenomenological constraints and will be tested in the near future at the LHC experiments with collider energy upgrade and by the future direct dark matter detection experiments.

4 Conclusion

The long-sought after Higgs boson of the Standard Model was discovered at the LHC by the ATLAS and CMS experiments through a variety of decay channels. Because the SM-like Higgs boson mass is predicted in the MSSM as a function of stop masses, the observed mass of 125-126 GeV has a great impact on the MSSM. In particular, it requires a relatively large stop mass. In the context of the CMSSM-like parameterization, the sfermion masses are found to be as large as $1-10$ TeV, and the discovery of (colored) sparticles at the LHC could be very challenging. On the other hand, the muon $g-2$ has been precisely measured, and the observed data shows more than 3σ deviation from the Standard Model prediction. This indicates that new physics below the TeV scale might exist, such that the associated new particles give rise to additional contributions to the muon $g-2$. The MSSM is a prime candidate for this new physics, however relatively light sparticles (neutralino, charginos and sleptons) with masses less than 1 TeV are required to account for the muon $g-2$ data.

We have attempted to reconcile these two results in a SU(5) inspired extension of the CMSSM parameterization for the soft SUSY breaking terms. In our setup, $m_{\bar{5}}$ and m_{10}, as well as soft masses^2 of the Higgs doublets, are taken as free parameters. With this generalization of the CMSSM, we have performed random parameter scans and examined a variety of phenomenological constraints including the observed Higgs boson mass of around 125 GeV, the muon $g-2$, the WMAP9 results for neutralino dark matter abundance, and the observations of rare B-meson decays. We have identified parameter regions which satisfy all the constraints. In particular, a soft mass^2 splitting between $\bar{5}$ and 10 matter fields, motivated by SU(5) GUT plays a crucial role in accommodating the Higgs boson mass and the muon $g-2$ data. We find $m_{\bar{5}} < m_{10}$ in the allowed parameter regions. The correct neutralino relic abundance is achieved by four different parameter sets, namely the sneutrino-neutralino coannihilation region, the stau-neutralino coannihilation region, the neutralino-Higgsino mixed region and the A-resonance region. For these regions, we have calculated the spin independent/dependent cross sections for the elastic scattering of neutralino dark matter with a nucleon. The resultant cross sections for these scenarios are shown to be within the reach of future experiments for direct dark matter searches. We have highlighted four

benchmark points which show characteristic particle mass spectra satisfying all the constraints (including the WMAP9 and Planck2013 bounds at 5σ) and can be tested in the near future at the LHC and by the dark matter direct detection experiments.

Acknowledgement

We would like to thank Ilia Gogoladze and Azar Mustafayev for useful discussions. This work is supported in part by the DOE Grant No. DE-FG02-10ER41714 (N.O.) and No. DE-FG02-91ER40626 (S.R and Q.S). This work used the Extreme Science and Engi- neering Discovery Environment (XSEDE), which is supported by the National Science Foundation grant number OCI-1053575

References

[1] G. Aad *et al.* [ATLAS Collaboration], Phys. Lett. B **716**, 1 (2012).

[2] S. Chatrchyan *et al.* [CMS Collaboration], Phys. Lett. B **716**, 30 (2012); arXiv:1303.4571 [hep-ex].

[3] See, for example, I. Gogoladze, Q. Shafi and C. S. Un, JHEP **1208**, 028 (2012); A. Arbey, M. Battaglia, A. Djouadi, F. Mahmoudi and J. Quevillon, Phys. Lett. B **708**, 162 (2012); P. Draper, P. Meade, M. Reece and D. Shih, Phys. Rev. D **85**, 095007 (2012); M. Carena, S. Gori, N. R. Shah and C. E. M. Wagner, JHEP **1203**, 014 (2012); M. Kadastik, K. Kannike, A. Racioppi and M. Raidal, JHEP **1205**, 061 (2012); U. Ellwanger, JHEP **1203**, 044 (2012); S. Akula, B. Altunkaynak, D. Feldman, P. Nath and G. Peim, Phys. Rev. D **85**, 075001 (2012); J. F. Gunion, Y. Jiang and S. Kraml, Phys. Lett. B **710**, 454 (2012); J. L. Evans, M. Ibe, S. Shirai and T. T. Yanagida, Phys. Rev. D **85**, 095004 (2012); S. F. King, M. Muhlleitner and R. Nevzorov, Nucl. Phys. B **860**, 207 (2012); Z. Kang, J. Li and T. Li, JHEP **1211**, 024 (2012) ; L. Aparicio, D. G. Cerdeno and L. E. Ibanez, JHEP **1204**, 126 (2012); J. Ellis, K. A. Olive and K. A. Olive, Eur. Phys. J. C **72**, 2005 (2012); H. Baer, V. Barger and A. Mustafayev, Phys. Rev. D **85**, 075010 (2012); H. Baer, V. Barger and A. Mustafayev, JHEP **1205**, 091 (2012); J. -J. Cao, Z. -X. Heng, J. M. Yang, Y. -M. Zhang and J. -Y. Zhu, JHEP **1203**, 086 (2012); F. Boudjema and G. D. La Rochelle, Phys. Rev. D **86**, 015018 (2012); D. A. Vasquez, G. Belanger, C. Boehm, J. Da Silva, P. Richardson and C. Wymant, Phys. Rev. D **86**, 035023 (2012); U. Ellwanger and C. Hugonie, Adv. High Energy Phys. **2012**, 625389 (2012); H. Baer, V. Barger, P. Huang and X. Tata, JHEP **1205**, 109 (2012); I. Gogoladze, Q. Shafi and C. S. Un, JHEP **1207**, 055 (2012); M. Hindmarsh and D. R. T. Jones, arXiv:1203.6838

[hep-ph]; M. A. Ajaib, I. Gogoladze, F. Nasir and Q. Shafi, Phys. Lett. B **713**, 462 (2012); J. L. Evans, M. Ibe and T. T. Yanagida, Phys. Rev. D **86**, 015017 (2012); T. Basak and S. Mohanty, Phys. Rev. D **86**, 075031 (2012); M. Badziak, E. Dudas, M. Olechowski and S. Pokorski, JHEP **1207**, 155 (2012); N. Okada, arXiv:1205.5826 [hep-ph]; E. Dudas, Y. Mambrini, A. Mustafayev and K. A. Olive, Eur. Phys. J. C **72**, 2138 (2012); M. Badziak, Mod. Phys. Lett. A **27**, 1230020 (2012); G. Altarelli, arXiv:1206.1476 [hep-ph]; P. Athron, S. F. King, D. J. Miller, S. Moretti, and R. Nevzorov, Phys. Rev. D **86**, 095003 (2012); A. Arbey, M. Battaglia, A. Djouadi, and F. Mahmoudi, JHEP **1209**, 107 (2012); E. Hardy, J. March-Russell and J. Unwin, JHEP **1210**, 072 (2012); S. Akula, P. Nath and G. Peim, Phys. Lett. B **717**, 188 (2012); J. Cao, Z. Heng, J. M. Yang, and J. Zhu, JHEP **1210**, 079 (2012); M. Hirsch, F. R. Joaquim and A. Vicente JHEP **1211**, 105 (2012); K. J. Bae, T. H. Jung and H. D. Kim, Phys. Rev. D **87**, 015014 (2013); K. Agashe, Y. Cui, and R. Franceschini, JHEP **1302**, 031 (2013); M. Badziak, S. Krippendorf, H. P. Nilles, and M. W. Winkler, JHEP **1303**, 094 (2013); N. Okada and H. M. Tran, Phys. Rev. D **87**, 035024 (2013).

[4] G. W. Bennett *et al.* [Muon G-2 Collaboration], Phys. Rev. D **73**, 072003 (2006).

[5] K. Hagiwara, A. D. Martin, D. Nomura, and T. Teubner, Phys. Lett. B **649**, 173 (2007); Chin. Phys. C **34**, 728 (2010); J. Phys. G **38**, 085003 (2011).

[6] J. L. Lopez, D. V. Nanopoulos, X. Wang and , Phys. Rev. D **49**, 366 (1994); U. Chattopadhyay, P. Nath and , Phys. Rev. D **53**, 1648 (1996); T. Moroi, Phys. Rev. D **53**, 6565 (1996) [Erratum-ibid. D **56**, 4424 (1997)].

[7] S. Profumo, Phys. Rev. D **68**, 015006 (2003); B. Ananthanarayan and P. N. Pandita, Int. J. Mod. Phys. A **22**, 3229 (2007) ; I. Gogoladze, R. Khalid, N. Okada, and Q. Shafi, Phys. Rev. D **79**, 095022 (2009).

[8] S. Mohanty, S. Rao, and D. P. Roy, arXiv:1303.5830 [hep-ph]; S. Akula and P. Nath, arXiv:1304.5526 [hep-ph].

[9] M. Ibe, S. Matsumoto, T. T. Yanagida and N. Yokozaki, JHEP **1303**, 078 (2013) [arXiv:1210.3122 [hep-ph]].

[10] H. Baer, F. E. Paige, S. D. Protopopescu and X. Tata, arXiv:hep-ph/0001086.

[11] J. Hisano, H. Murayama, and T. Yanagida, Nucl. Phys. **B402** (1993) 46. Y. Yamada, Z. Phys. **C60** (1993) 83; J. L. Chkareuli and I. G. Gogoladze, Phys. Rev. D **58**, 055011 (1998).

[12] For recent discussions and additional references see V. Barger, D. Marfatia and A. Mustafayev, Phys. Lett. B **665**, 242 (2008); M. E. Gomez, S. Lola, P. Naranjo and J. Rodriguez-Quintero, arXiv:0901.4013 [hep-ph].

[13] D. M. Pierce, J. A. Bagger, K. T. Matchev, and R.-j. Zhang, Nucl. Phys. **B491** (1997) 3.

[14] L. E. Ibanez and G. G. Ross, Phys. Lett. **B110** (1982) 215; K. Inoue, A. Kakuto, H. Komatsu and S. Takeshita, Prog. Theor. Phys. **68**, 927 (1982) [Erratum-ibid. **70**, 330 (1983)]; L. E. Ibanez, Phys. Lett. **B118** (1982) 73; J. R. Ellis, D. V. Nanopoulos, and K. Tamvakis, Phys. Lett. **B121** (1983) 123; L. Alvarez-Gaume, J. Polchinski, and M. B. Wise, Nucl. Phys. **B221** (1983) 495.

[15] K. Nakamura *et al.* [Particle Data Group], J. Phys. G **37**, 075021 (2010).

[16] [Tevatron Electroweak Working Group and CDF Collaboration and D0 Collab], arXiv:0903.2503 [hep-ex].

[17] I. Gogoladze, R. Khalid, S. Raza and Q. Shafi, JHEP **1106** (2011) 117.

[18] G. Belanger, F. Boudjema, A. Pukhov and R. K. Singh, JHEP **0911**, 026 (2009); H. Baer, S. Kraml, S. Sekmen and H. Summy, JHEP **0803**, 056 (2008).

[19] H. Baer and M. Brhlik, *Phys. Rev.* **D 55** (1997) 4463; H. Baer, M. Brhlik, D. Castano and X. Tata, *Phys. Rev.* **D 58** (1998) 015007;

[20] K. Babu and C. Kolda, *Phys. Rev. Lett.* **84** (2000) 228; A. Dedes, H. Dreiner and U. Nierste, *Phys. Rev. Lett.* **87** (2001) 251804; J. K. Mizukoshi, X. Tata and Y. Wang, *Phys. Rev.* **D 66** (2002) 115003.

[21] D. Eriksson, F. Mahmoudi and O. Stal, *J. High Energy Phys.* **0811** (2008) 035.

[22] R. Aaij *et al.* [LHCb Collaboration], Phys. Rev. Lett. **110**, 021801 (2013).

[23] T. Aaltonen *et al.* [CDF Collaboration], Phys. Rev. Lett. **100**, 101802 (2008).

[24] Y. Amhis *et al.* [Heavy Flavor Averaging Group Collaboration], arXiv:1207.1158 [hep-ex].

[25] D. Asner *et al.* [Heavy Flavor Averaging Group Collaboration], arXiv:1010.1589 [hep-ex].

[26] G. Hinshaw *et al.* [WMAP Collaboration], arXiv:1212.5226 [astro-ph.CO].

[27] P. A. R. Ade *et al.* [Planck Collaboration], arXiv:1303.5076 [astro-ph.CO].

[28] E. Aprile *et al.* [XENON100 Collaboration], Phys. Rev. Lett. **109**, 181301 (2012) [arXiv:1207.5988 [astro-ph.CO]].

[29] The XENON Dark Matter Project
`http://xenon.astro.columbia.edu/talks/aprile_ucla_dm2010.pdf/`

[30] `http://cdms.berkeley.edu/APS_Panofsky_130413_Cabrera.pdf/`

[31] T. Tanaka *et al.* [Super-Kamiokande Collaboration], Astrophys. J. **742**, 78 (2011) [arXiv:1108.3384 [astro-ph.HE]].

[32] R. Abbasi *et al.* [ICECUBE Collaboration], Phys. Rev. Lett. **102**, 201302 (2009) [arXiv:0902.2460 [astro-ph.CO]].

[33] H. Baer, V. Barger, A. Lessa and X. Tata, arXiv:1207.4846 [hep-ph].

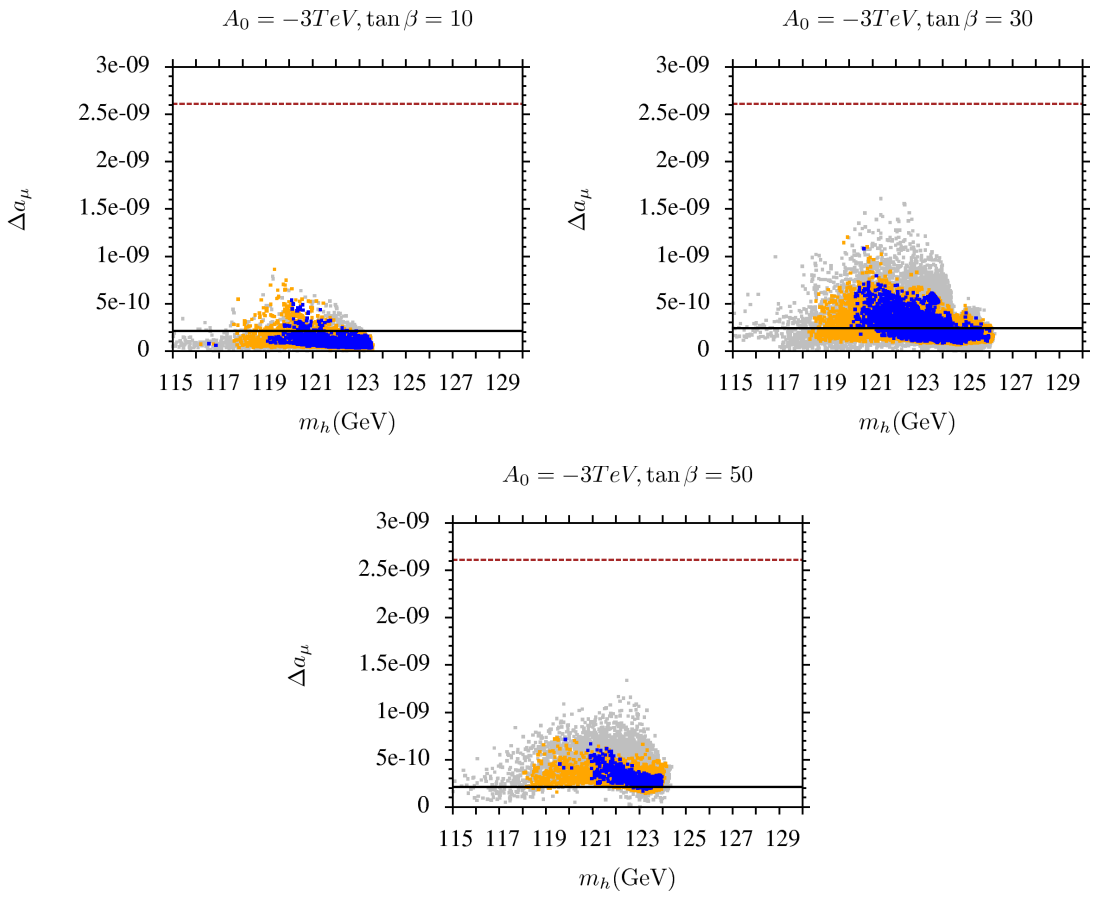


Figure 1: Plots in (Δa_μ, m_h)-plane. Gray points satisfy the requirements of REWSB and neutralino LSP. Orange points satisfy mass bounds and B-physics bounds. Blue points are subset of the orange points and represent solutions satisfying the WMAP9 bounds at 5σ and $m_{\tilde{g}}$, $m_{\tilde{d}_R} \geq 1$ TeV.

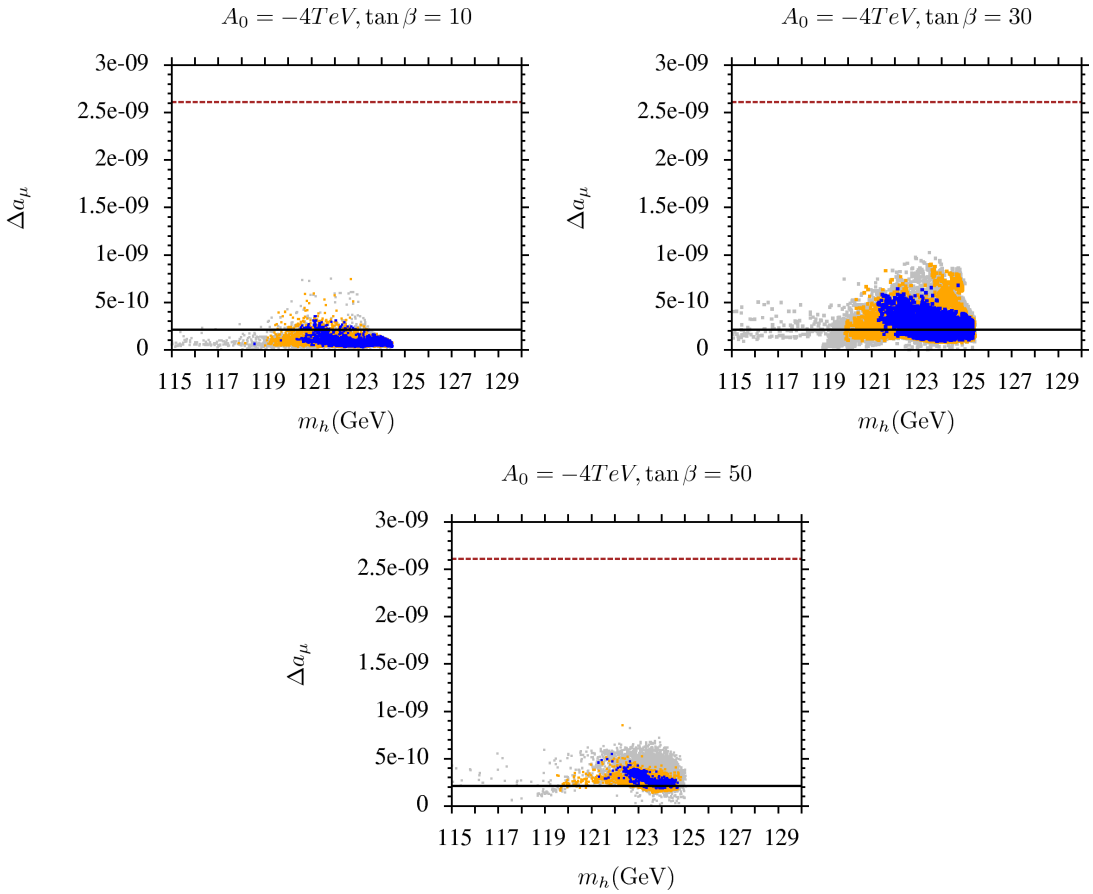


Figure 2: Color coding same as in Fig. 1, with $A_0 = -4$ TeV.

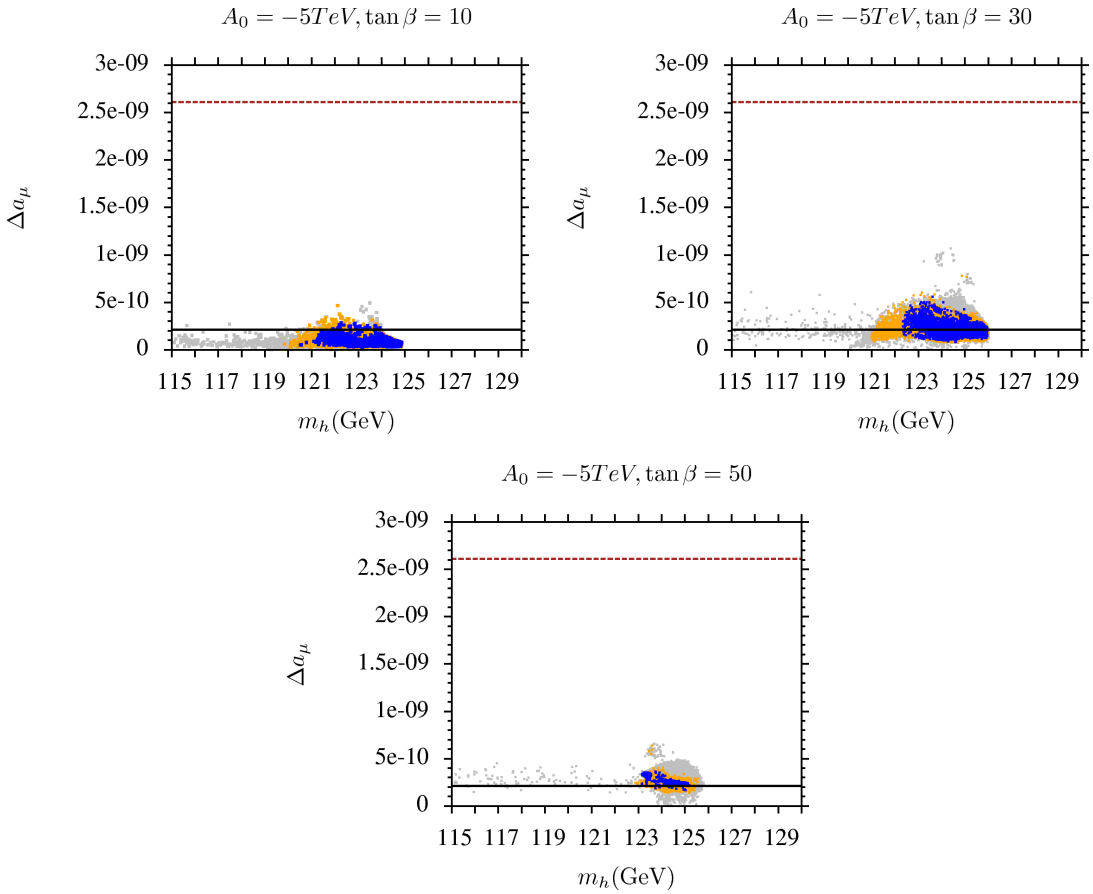


Figure 3: Color coding same as in Fig. 1, for $A_0 = -5$ TeV.

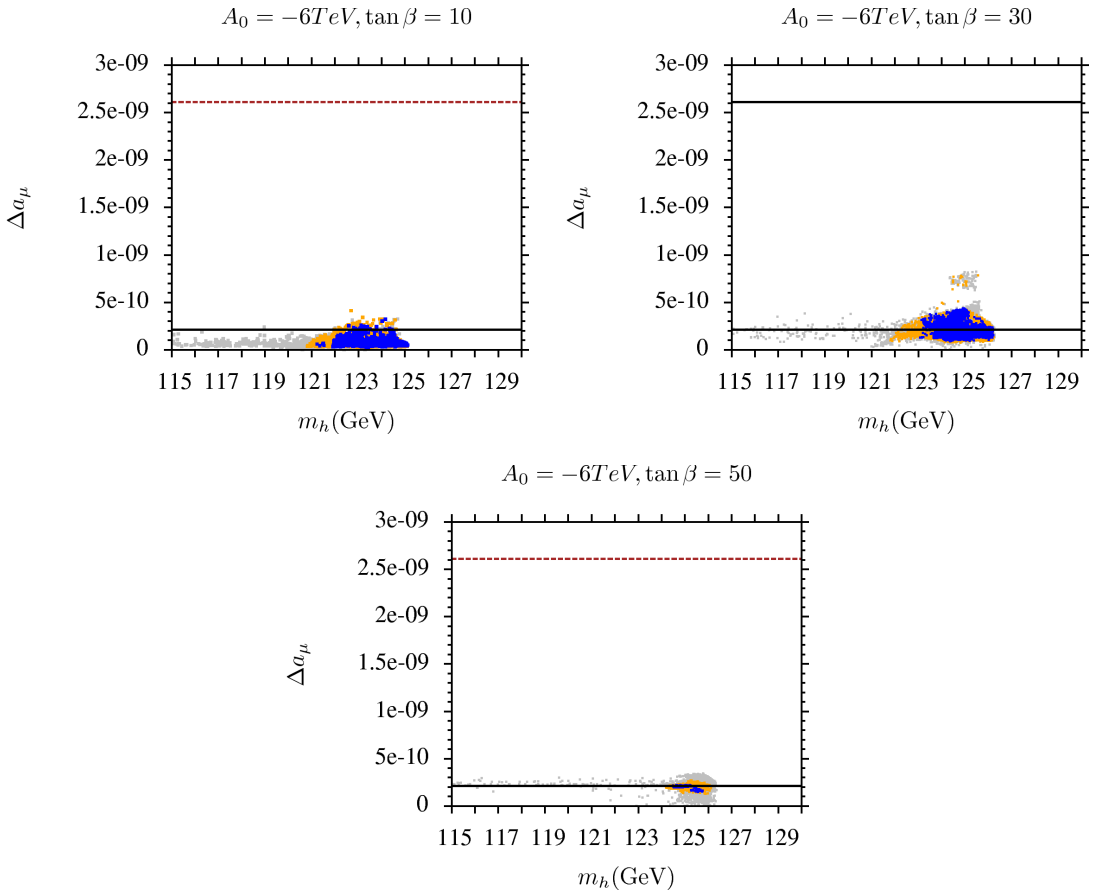


Figure 4: Color coding same as in Fig. 1, for $A_0 = -6$ TeV.

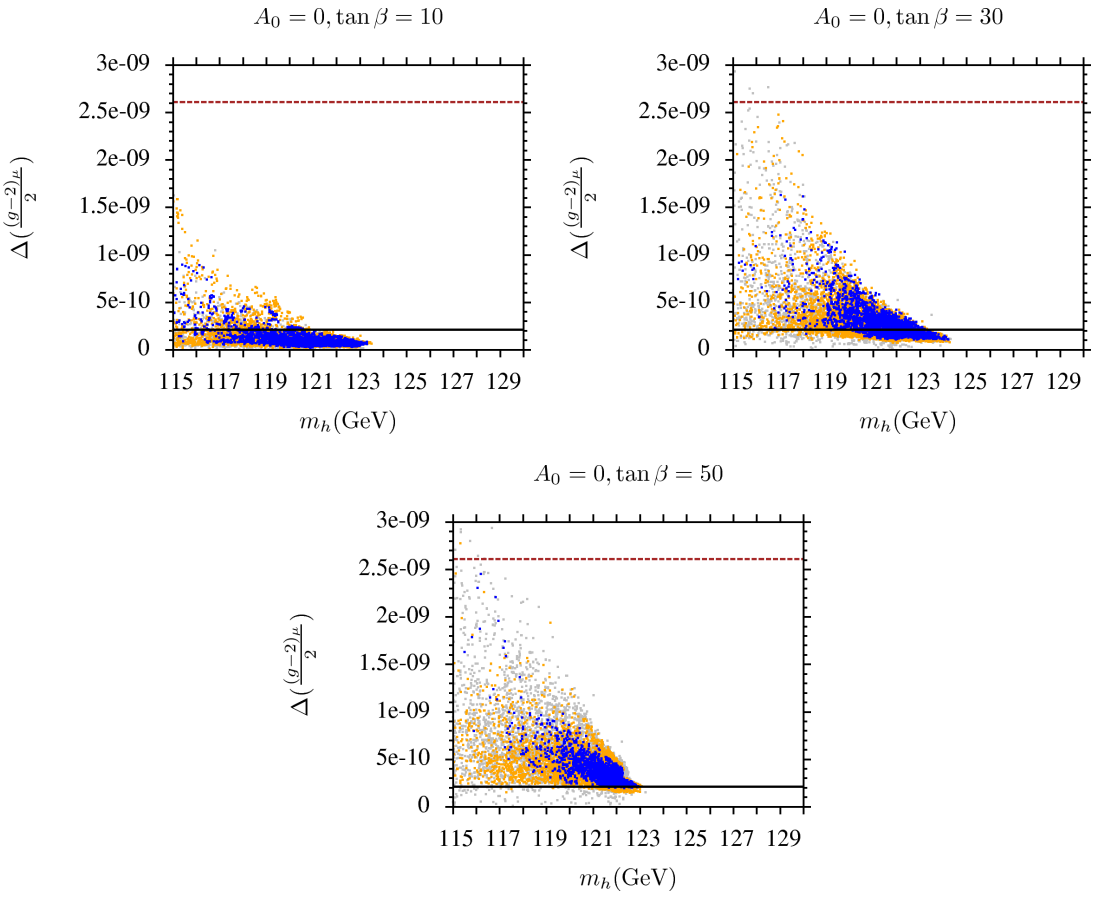


Figure 5: Color coding same as in Fig. 1, for $A_0 = 0$ TeV.

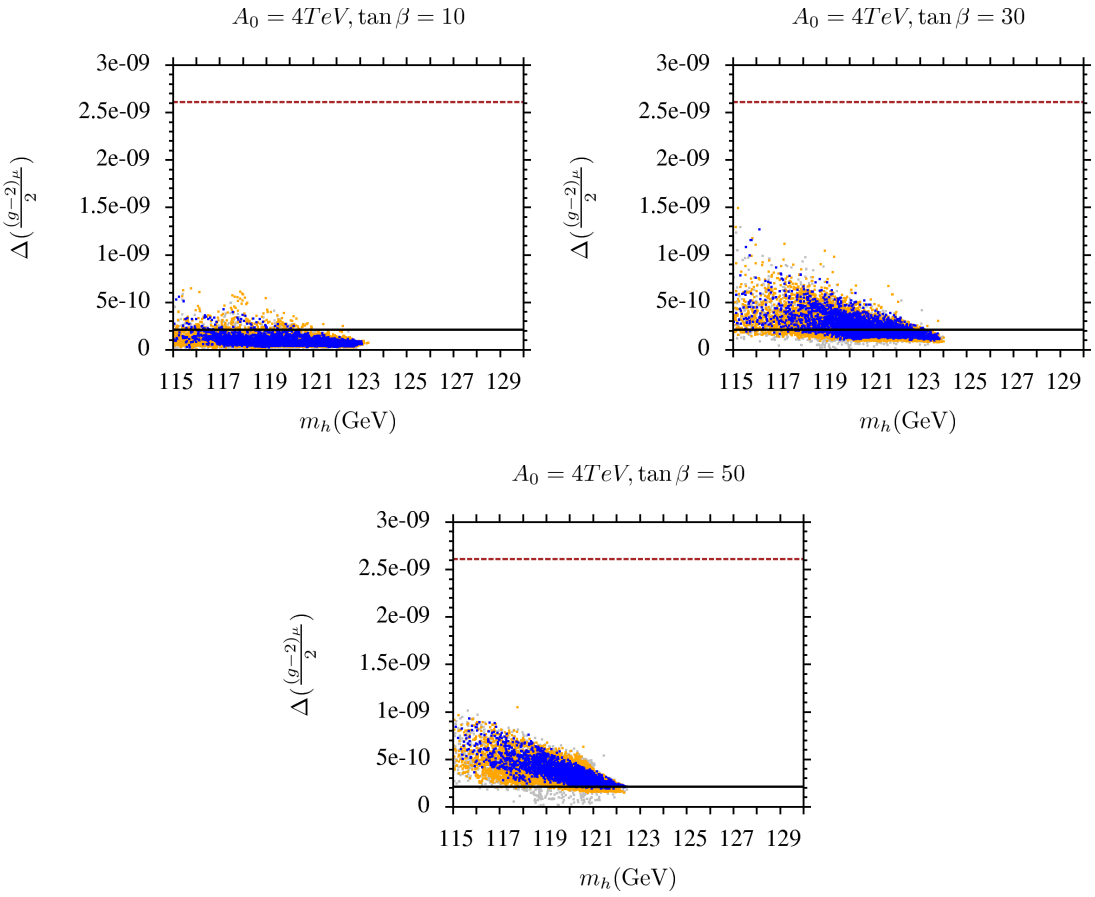


Figure 6: Color coding same as in Fig. 1, for $A_0 = 4$ TeV.

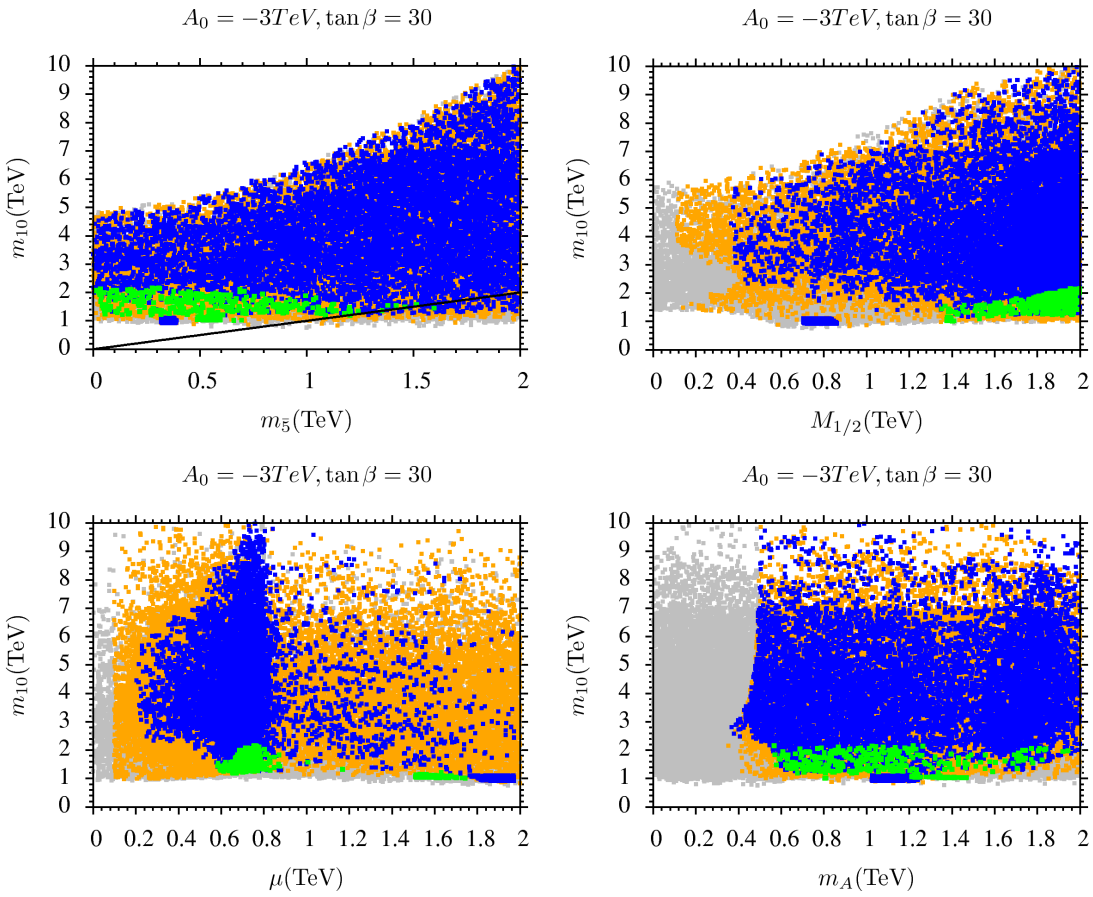


Figure 7: Plots in (m_{10}, $m_{\bar{5}}$)-plane, (m_{10}, $M_{1/2}$)-plane, ($m_{\bar{5}}$, $M_{1/2}$)-plane and (m_A, μ)-plane. Gray points satisfy the requirements of REWSB and neutralino LSP. Orange points satisfy mass bounds and B-physics bounds. Blue points are subset of the orange points and represent solutions satisfying the WMAP9 (5σ) bounds, 124 GeV $\leq m_h \leq$ 127 GeV, $m_{\tilde{g}}$, $m_{\tilde{d}_R} \gtrsim 1$ TeV. Green points are subset of the blue points and satisfy the 3σ bounds on Δa_μ.

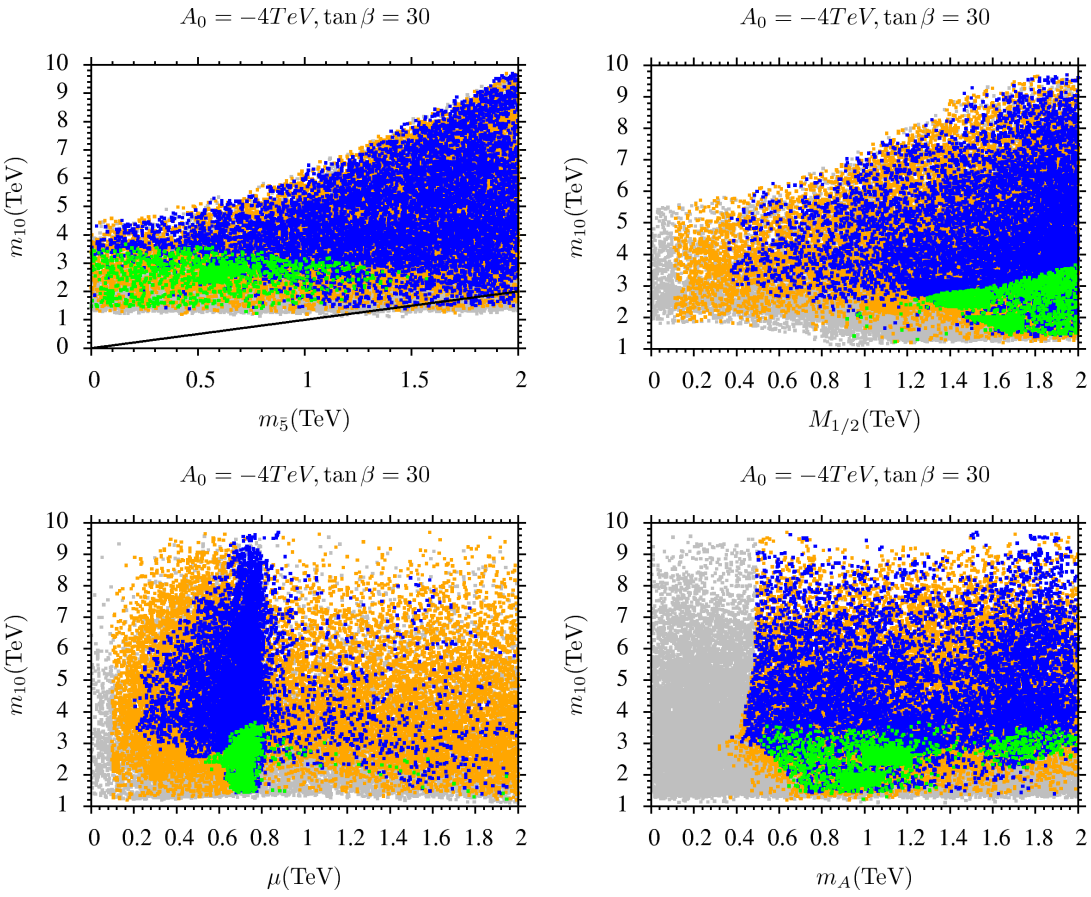


Figure 8: Color coding same as in Fig. 7, with $A_0 = -4$ TeV.

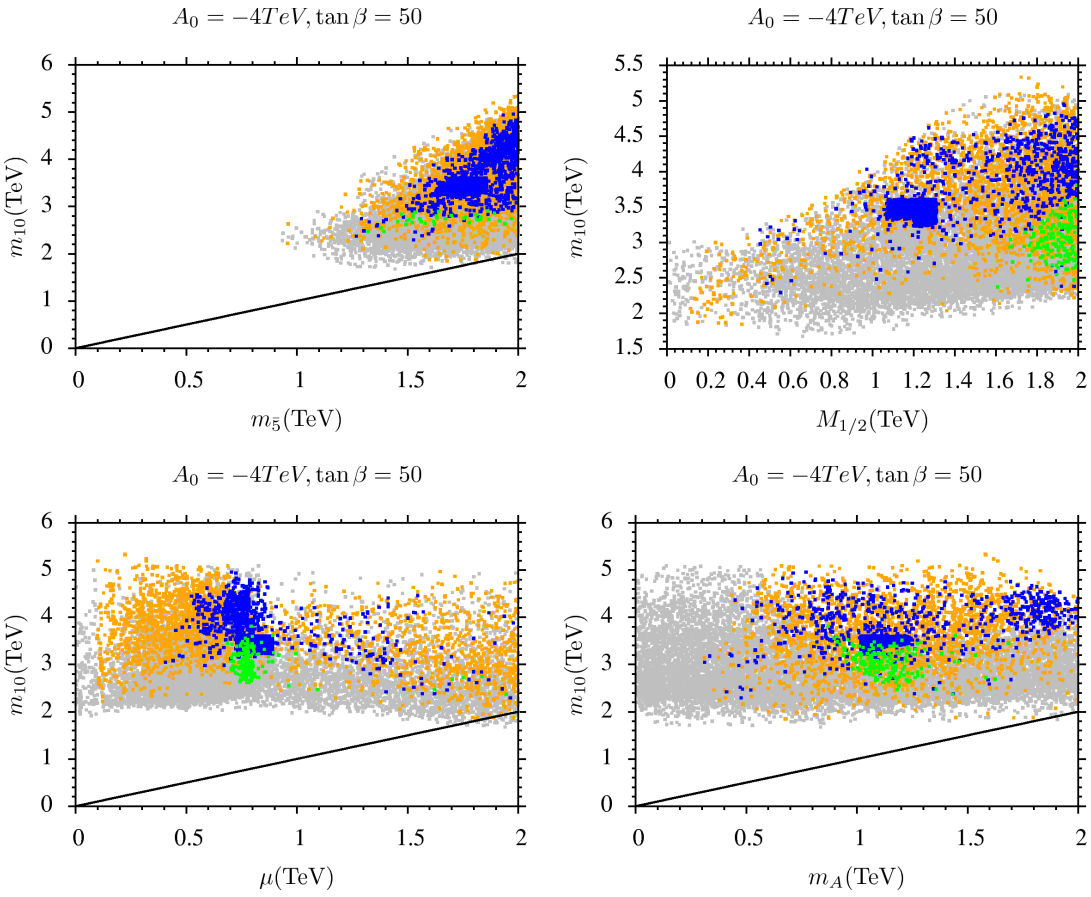


Figure 9: Color coding same as in Fig. 7, with $A_0 = -4$ TeV.

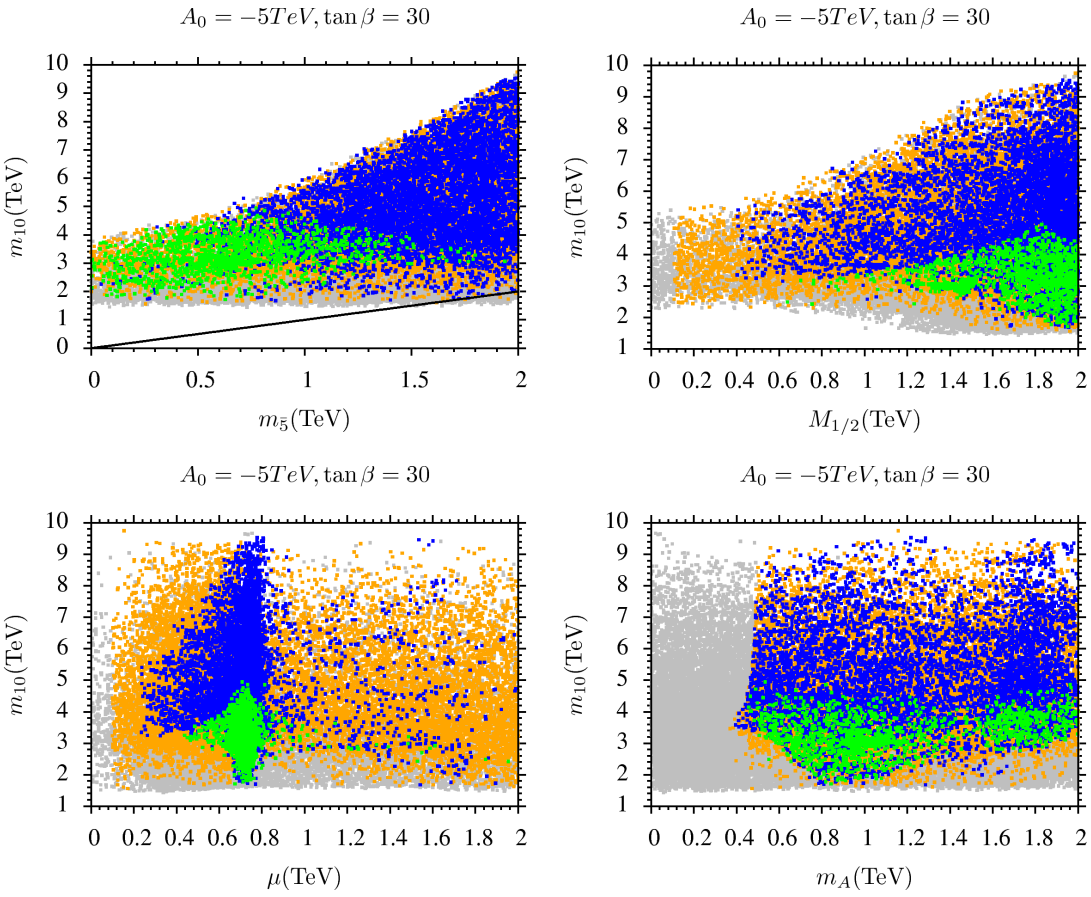


Figure 10: Color coding same as in Fig. 7, for $A_0 = -5$ TeV.

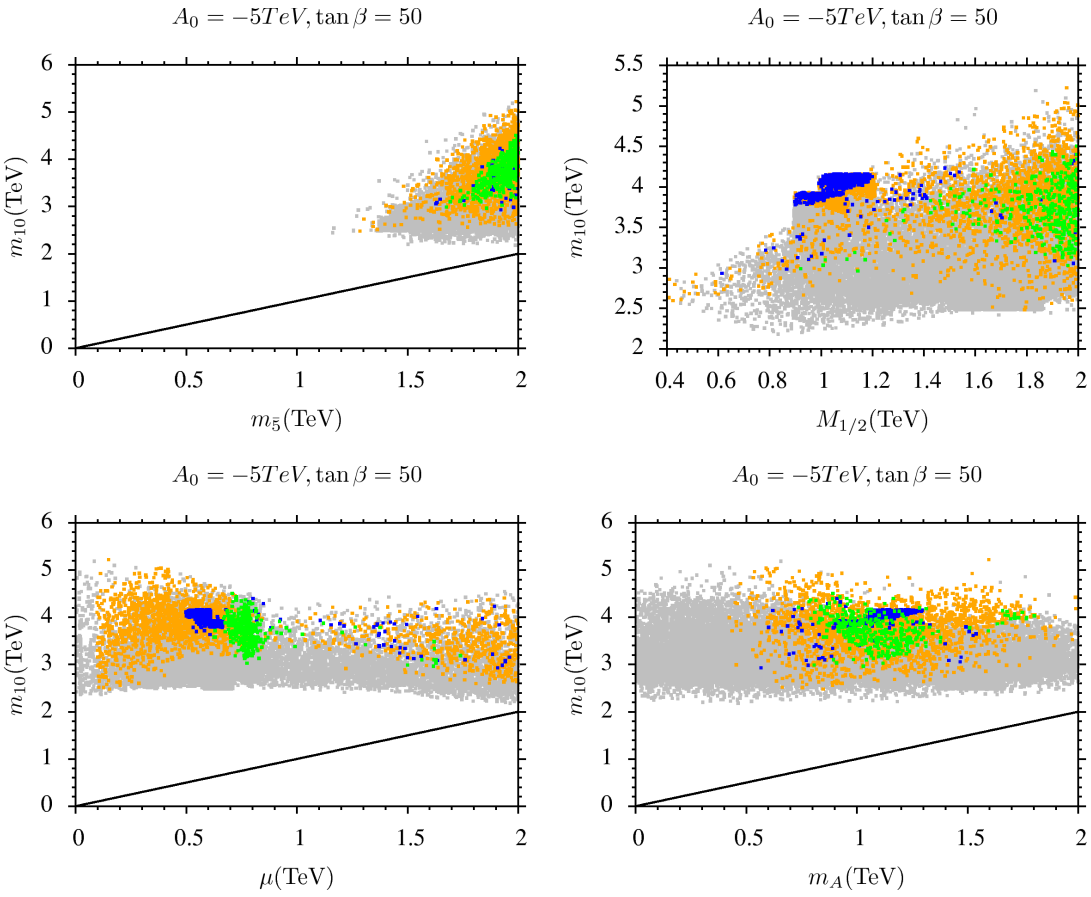


Figure 11: Color coding same as in Fig. 7, for $A_0 = -5$ TeV.

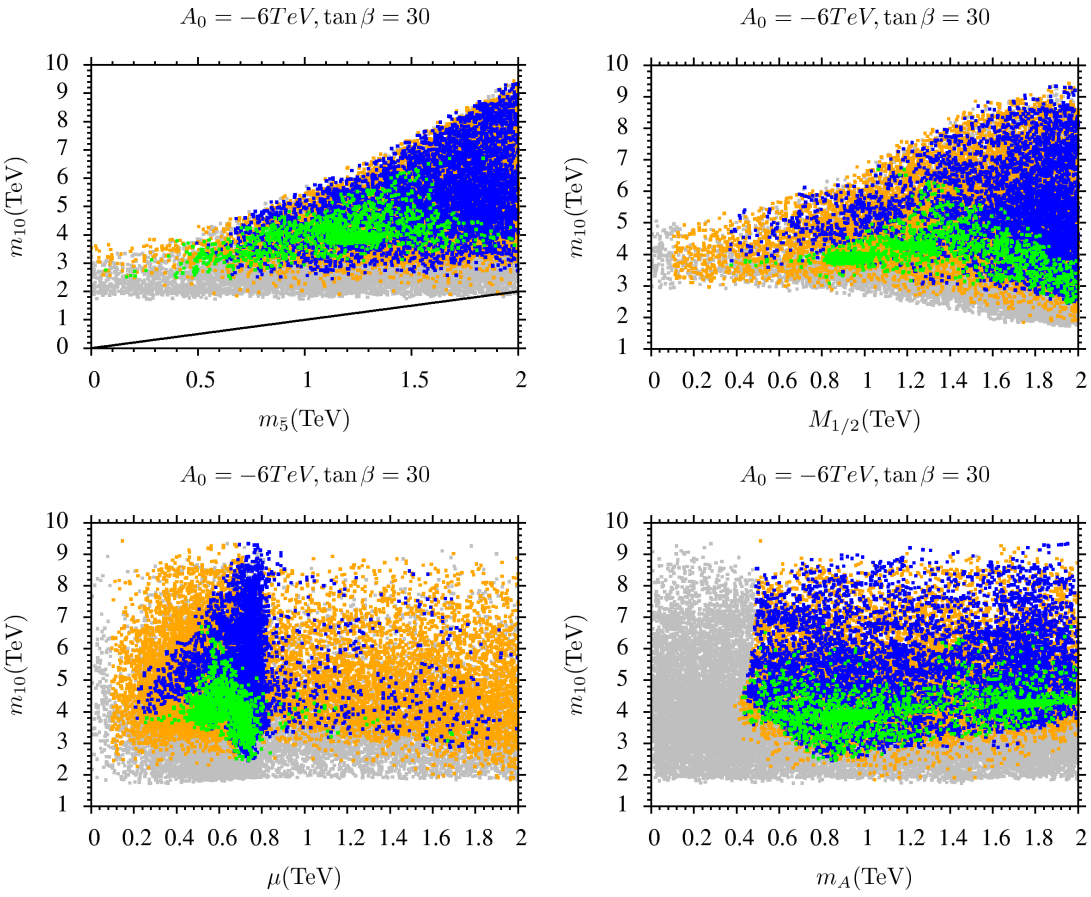


Figure 12: Color coding same as in Fig. 7, for $A_0 = -6$ TeV.

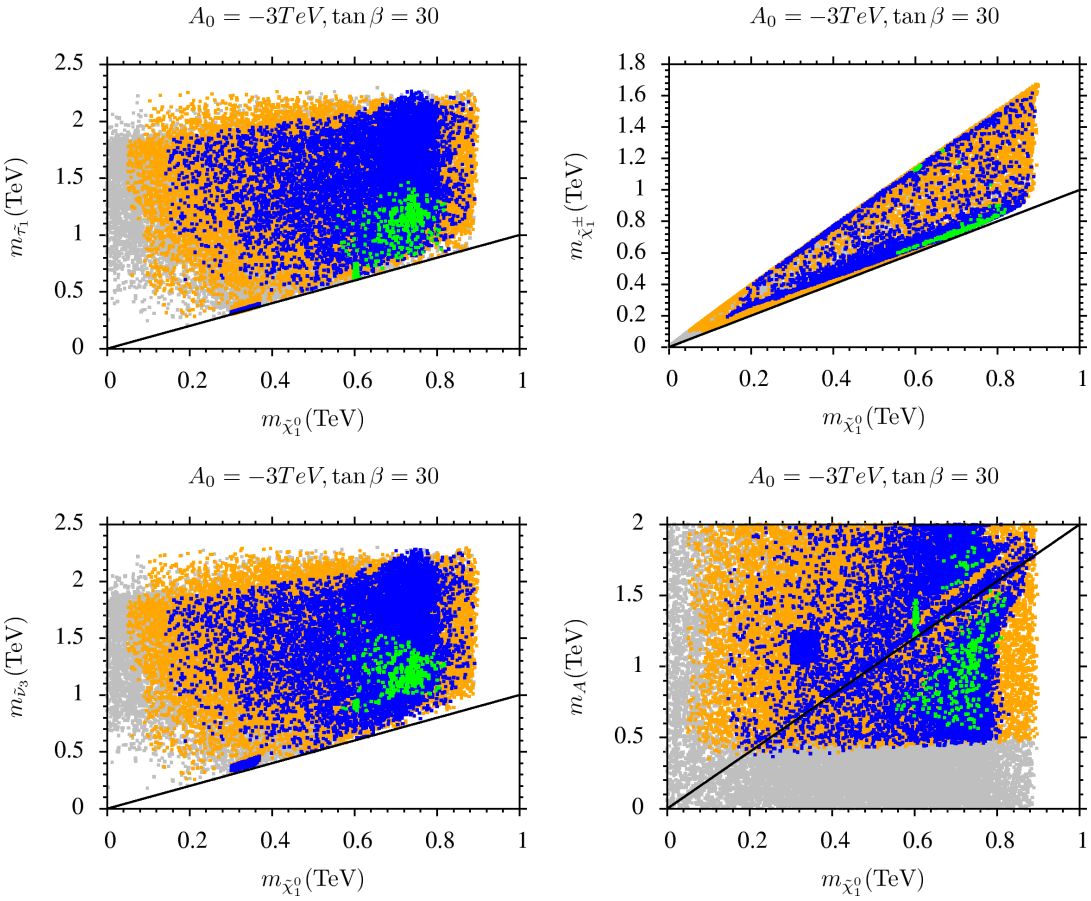


Figure 13: Results for $A_0 = -3$ TeV and $\tan\beta = 30$. Color coding same as in Fig. 7.

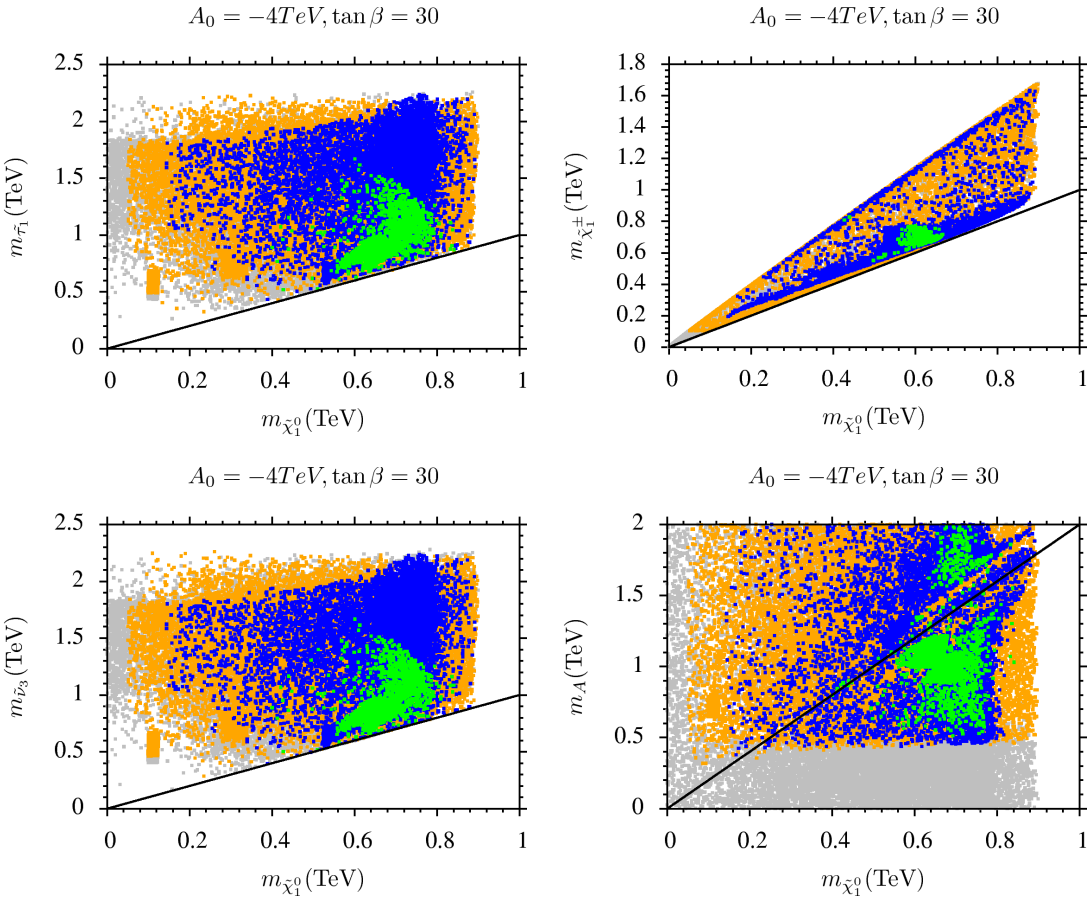


Figure 14: Color coding same as in Fig. 13, for $A_0 = -4$ TeV.

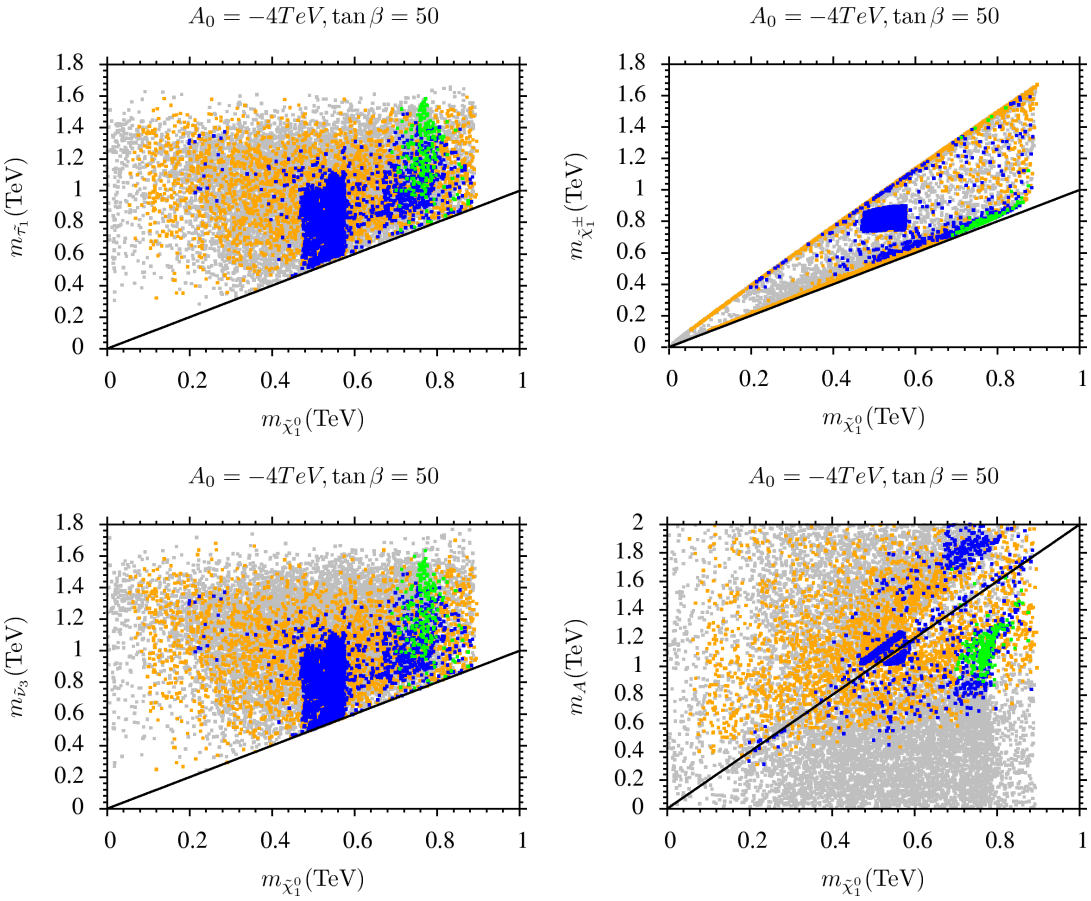


Figure 15: Color coding same as in Fig. 13, for $A_0 = -4$ TeV.

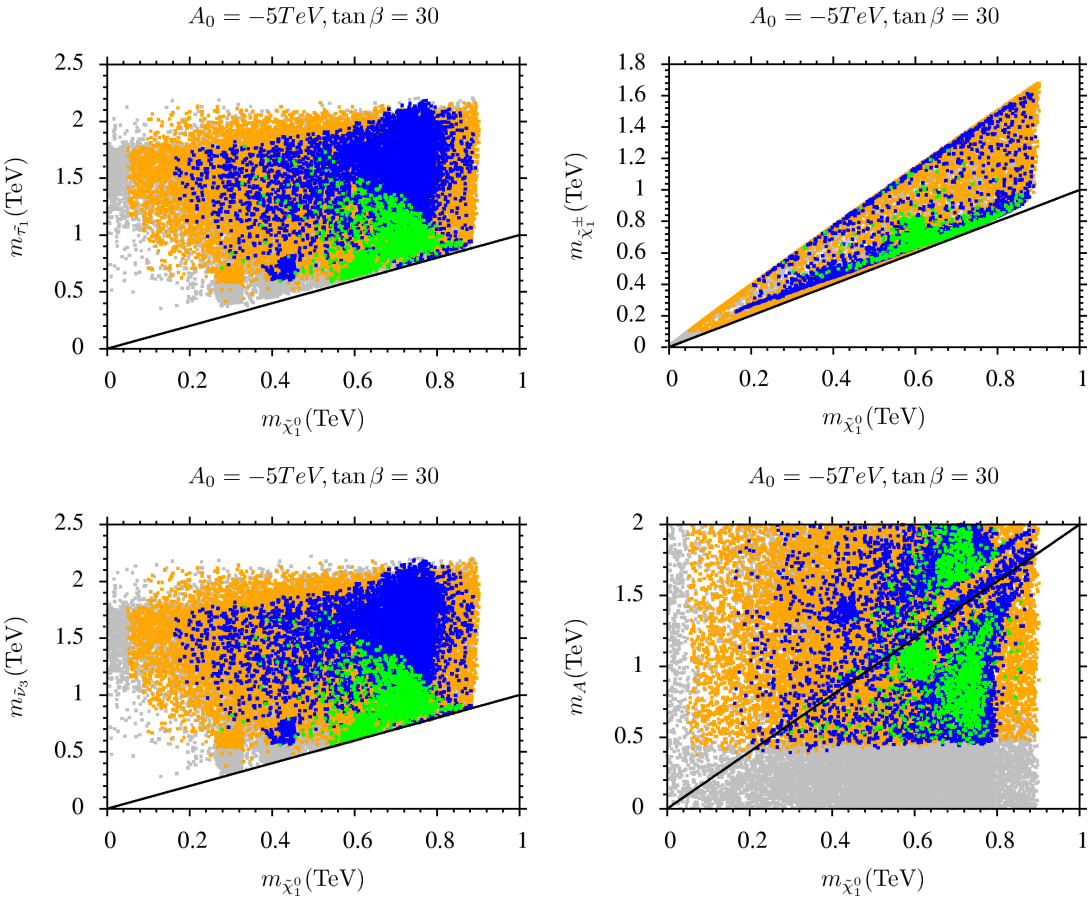


Figure 16: Color coding same as in Fig. 13, for $A_0 = -5$ TeV.

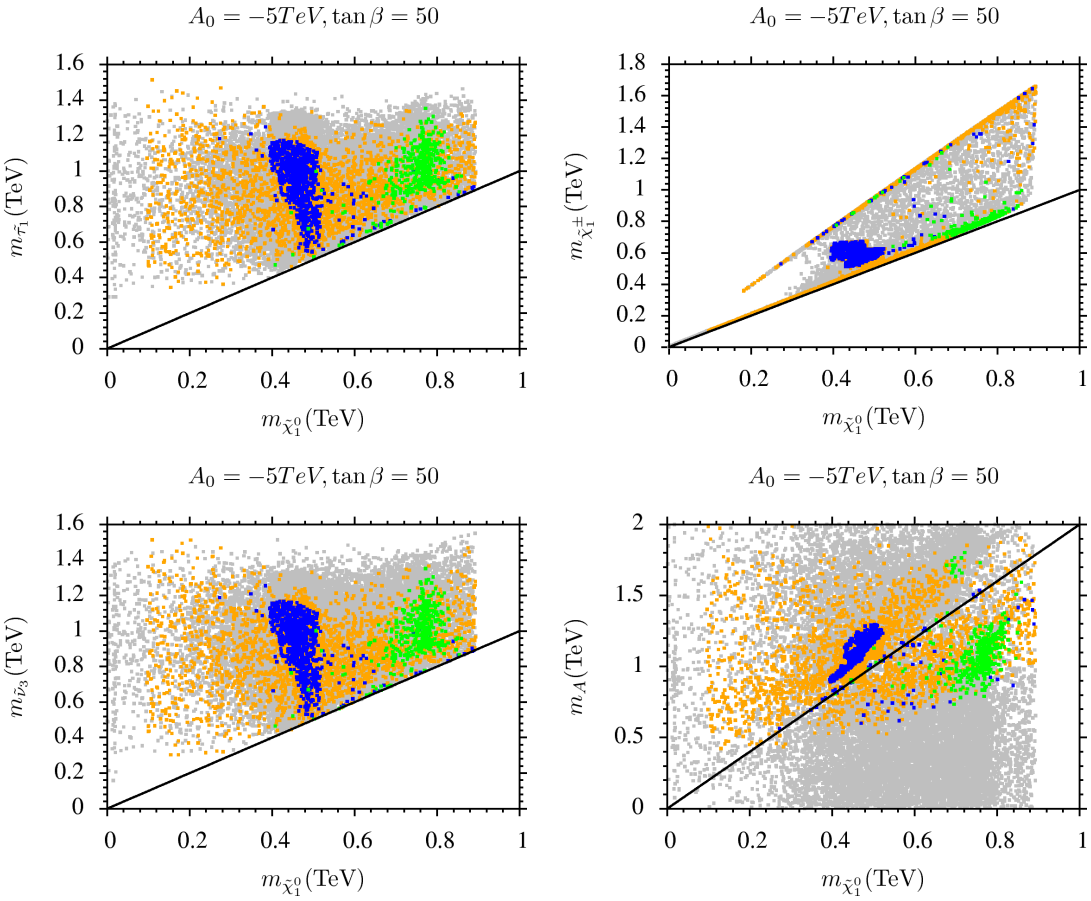


Figure 17: Color coding same as in Fig. 13, for $A_0 = -5$ TeV.

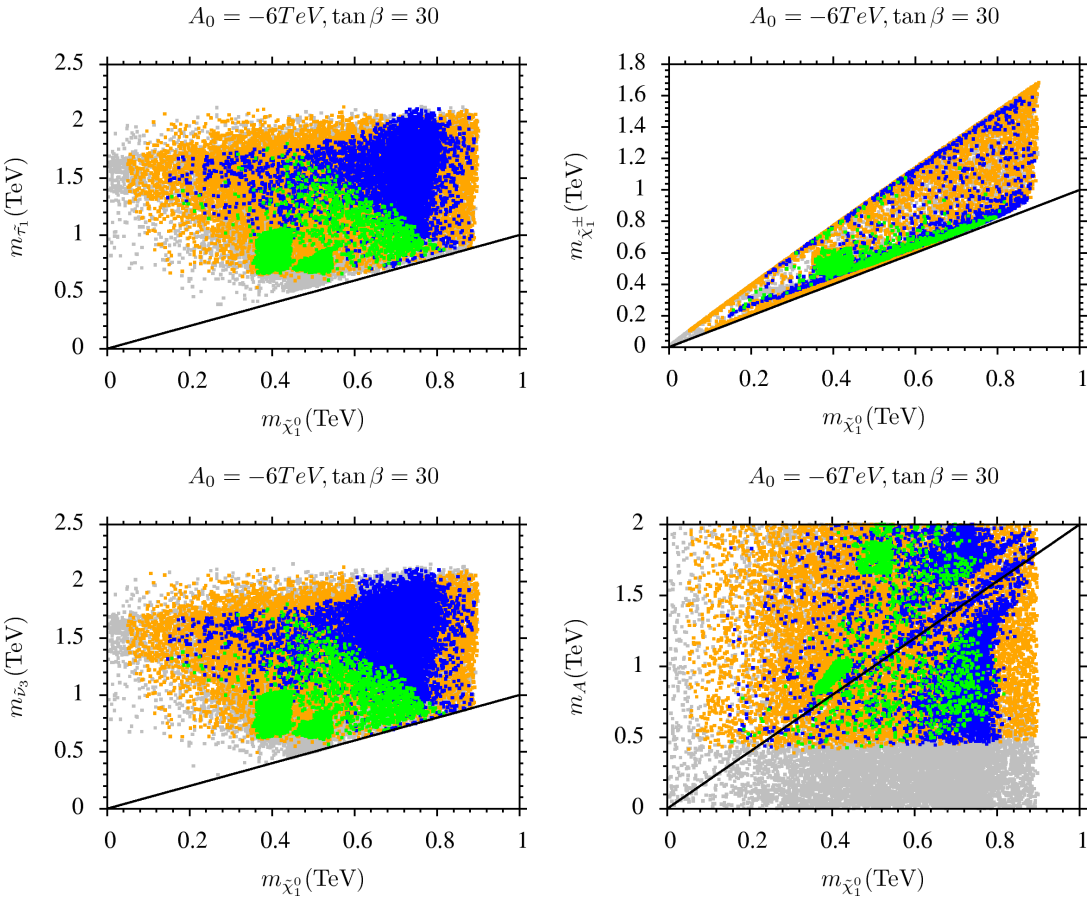


Figure 18: Color coding same as in Fig. 13, for $A_0 = -6$ TeV.

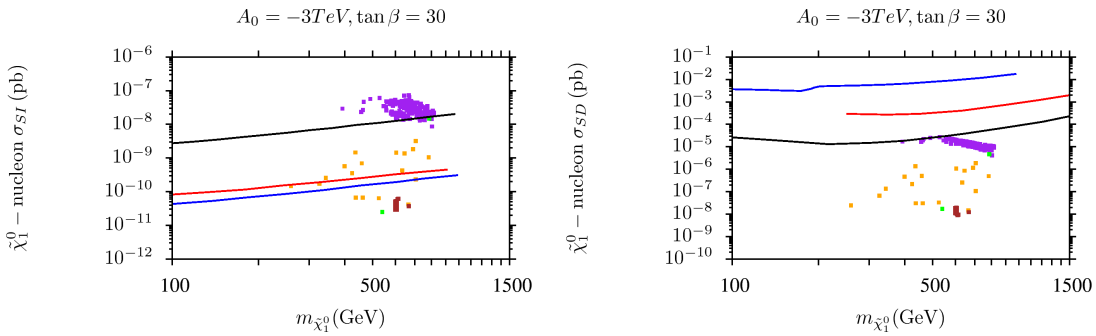


Figure 19: The SI and SD cross sections of neutralino elastic scattering with nucleon, along with the current and future bounds of direct and indirect dark matter detection experiments. All points satisfy the requirements of REWSB, neutralino LSP, mass bounds, B-physics bounds, the WMAP9 (5σ) bounds, Higgs boson mass and Δa_μ bound. Purple, green, orange and brown points respectively, represent the results in the bino-Higgsino mixed dark matter region, the sneutrino-neutralino coannihilation region, the A-resonance and the stau-neutralino coannihilation region. In the left panel, the black line represents the current upper bound set by XENON 100, while the blue (red) line represents future reach of XENON 1T (SuperCDMS). In the right panel, the current upper bounds set by Super-K (blue line) and IceCube DeepCore (red line) are shown. Future IceCube DeepCore bound is depicted by the black line.

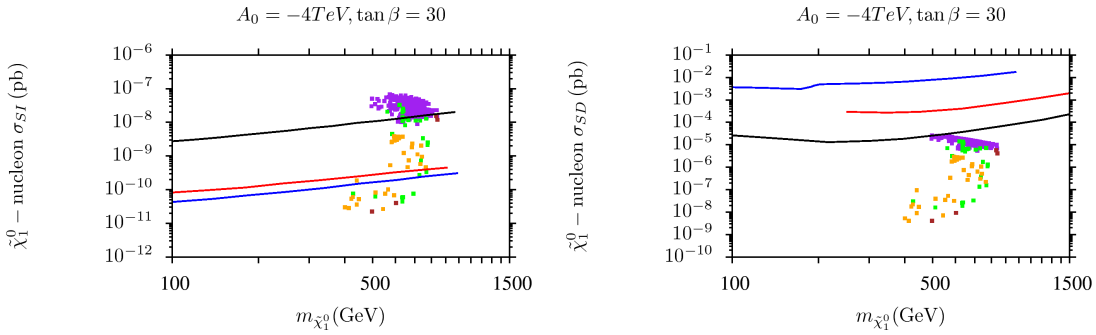


Figure 20: Color coding same as in Fig. 19, for $A_0 = -4$ TeV and $\tan\beta = 30$.

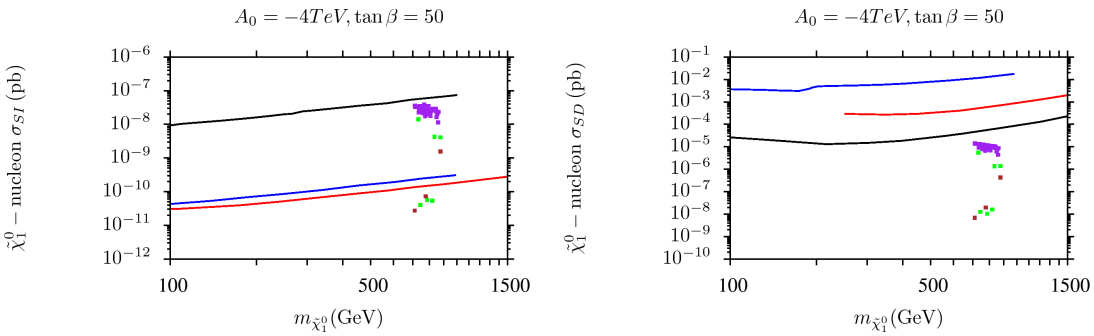


Figure 21: Color coding same as in Fig. 19, for $A_0 = -4$ TeV and $\tan\beta = 50$.

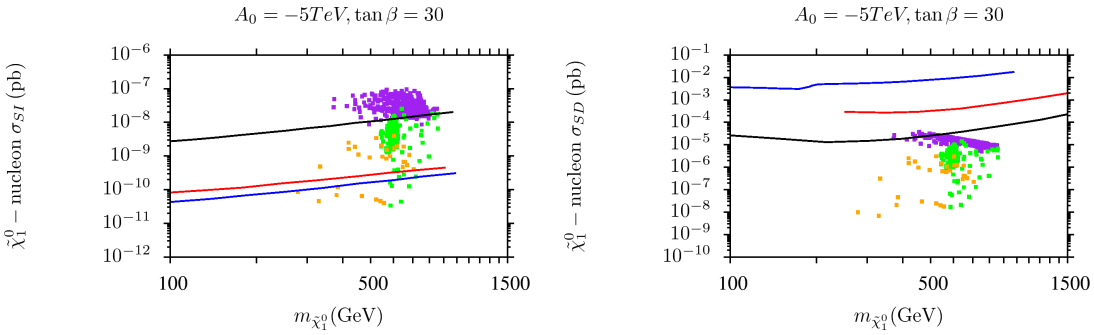


Figure 22: Color coding same as in Fig. 19, for $A_0 = -5$ TeV and $\tan\beta = 30$.

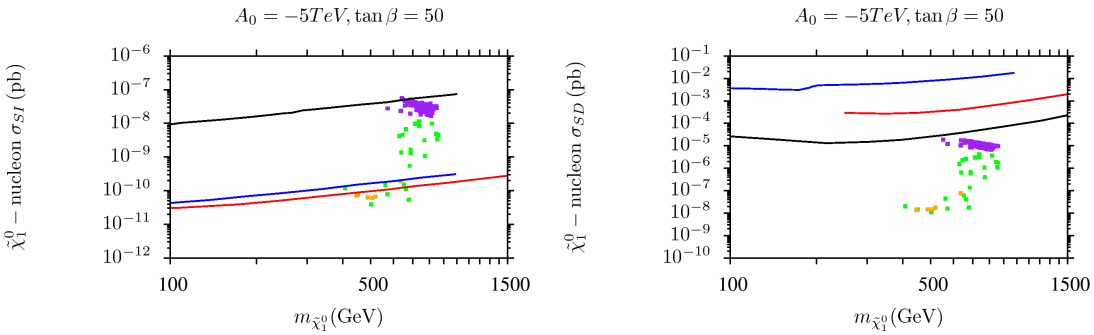


Figure 23: Color coding same as in Fig. 19, for $A_0 = -5$ TeV and $\tan\beta = 50$.

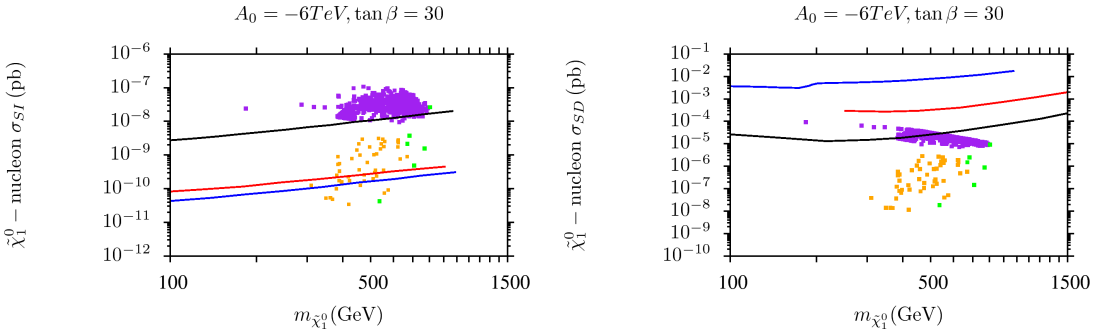


Figure 24: Color coding same as in Fig. 19, for $A_0 = -6$ TeV and $\tan\beta = 30$.

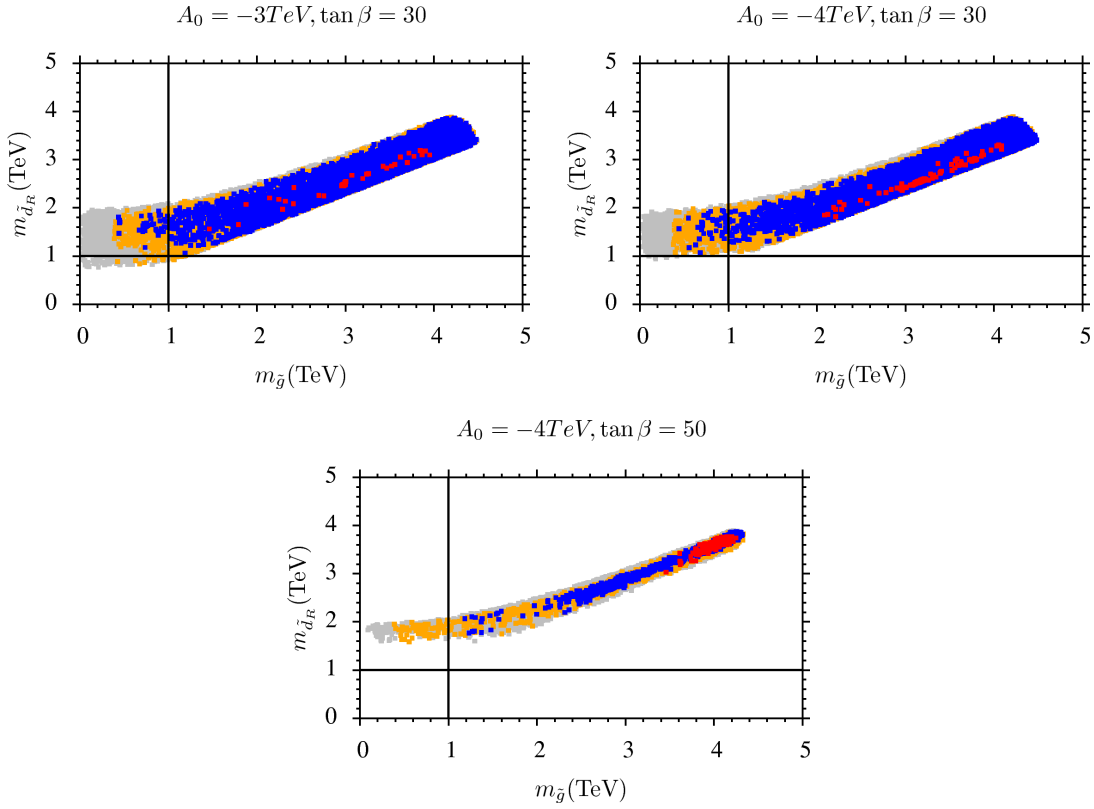


Figure 25: Plots in $(m_{\tilde{g}}, m_{\tilde{d}_R})$-plane. Gray points satisfy the requirements of REWSB and neutralino LSP. Orange points satisfy mass bounds and B-physics bounds. Blue points are subset of the orange points and represent solutions satisfying the WMAP9 (5σ) bounds, 124 GeV $\leq m_h \leq$ 127 GeV, $m_{\tilde{g}}$, $m_{\tilde{d}_R} \gtrsim 1$ TeV. Red points are a subset of the blue points and satisfy the 3σ bounds on Δa_μ and current upper bounds set by XENON 100.

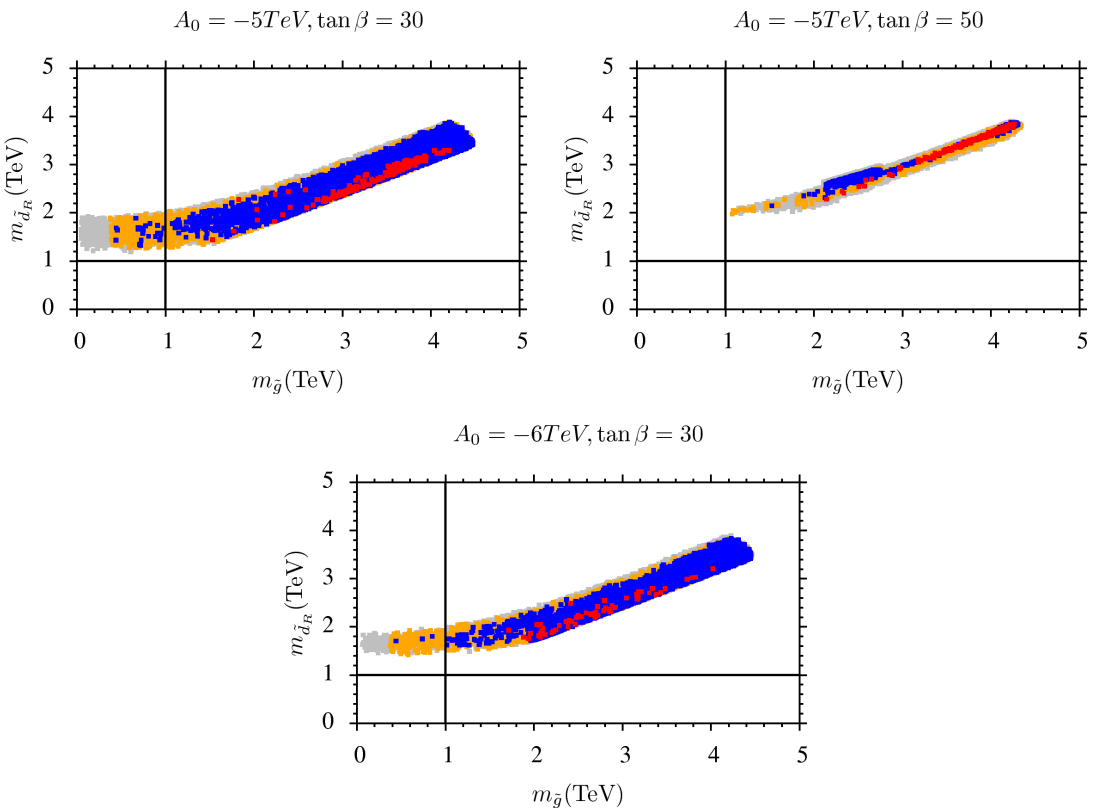


Figure 26: Color coding same as in Fig. 25 .

	Point 1	Point 2	Point 3	Point 4
m_{10}	1046	2382	2988	3788
$m_{\bar{5}}$	492.8	542.7	1675	1131
$M_{1/2}$	1381	1471	921.2	912.2
A_0	-3000	-4000	-5000	-6000
$\tan\beta$	30	30	50	30
μ	1556	697.8	1500	586.4
m_A	1340	1127	806.3	882.4
m_h	124	124.5	124	125
m_H	1349	1134	811	888
$m_{H^\pm}$	1351	1138	817	892
$m_{\tilde{g}}$	2970	3200	2146	2145
$m_{\tilde{\chi}^0_{1,2}}$	601,1126	632, 711	407, 776	398, 582
$m_{\tilde{\chi}^0_{3,4}}$	1560, 1567	716, 1218	1497, 1501	597, 788
$m_{\tilde{\chi}^\pm_{1,2}}$	1130,1567	719, 1201	776, 1504	591, 776
$m_{\tilde{u}_{L,R}}$	2882,2809	3701, 3677	3483, 3485	4161, 4229
$m_{\tilde{t}_{1,2}}$	1606,2306	1766, 2779	1415, 2294	1404, 2839
$m_{\tilde{d}_{L,R}}$	2884,2595	3702, 2717	3484, 2386	4162, 1931
$m_{\tilde{b}_{1,2}}$	2281,2351	2286, 2781	1272, 2282	921, 2848
$m_{\tilde{\nu}_1}$	1076	1206	1808	1409
$m_{\tilde{\nu}_3}$	880	822	501	690
$m_{\tilde{e}_{L,R}}$	1084,1077	1217, 2331	1810, 2959	1419, 3682
$m_{\tilde{\tau}_{1,2}}$	617,897	839, 1963	507, 1606	721, 3241
σ_{SI}(pb)	3.99×10^{-11}	1.17×10^{-8}	1.08×10^{-10}	2.45×10^{-9}
σ_{SD}(pb)	2.10×10^{-8}	1.25×10^{-5}	2.81×10^{-8}	4.11×10^{-6}
$\Omega_{CDM}h^2$	0.11	0.11	0.11	0.11
Δa_μ	2.76×10^{-10}	3.40×10^{-10}	3.16×10^{-10}	3.86×10^{-10}

Table 1: Benchmark points for $A_0 = -3, -4, -5, -6$ TeV and $\tan\beta = 30, 50$. Sparticle and Higgs masses are in GeV. These benchmark points satisfy all phenomenological constraints. Point 1, 2, 3 and 4 are chosen, respectively, from the stau-neutralino coannihilation region, the bino-Higgsino mixed dark matter region, the sneutrino-neutralino coannihilation region, and the A-resonance region.